Intrinsic Predictability of the Madden-Julian Oscillation

Wen-wen Tung

Department of Earth & Atmospheric Sciences
Purdue University, IN

wwtung@purdue.edu, P2.84

Jianbo Gao

PMB InTelliGence, LLC

Department of Mechanical and Manufacturing Engineering
Wright State University, OH

Acknowledgments:

K. Bowman, J. Gottschalck, J. Hu, Y. Lei, J.-L. F. Li, A. Majda, D. Waliser, and Y.-C. Wang

NSF CMMI-0825311 and 0826119

Reference: Tung et al., 2011, Detecting chaos in heavy-noise environment, *Phy. Rev. E*, **83**, DOI: 10.1103/PhysRevE.83.046210

OUTLINE

- Background and significance
- Adaptive filtering of MJO indices
  - The adaptive denoising algorithm
  - Bandpass filtering of MJO indices by LSAF
- Quantifying the intrinsic predictability of MJO
  - Brief introduction to chaotic dynamics
  - Characterizing chaos by scale-dependent Lyapunov exponent (SDLE)
  - Pseudo-ensemble approach based on SDLE
  - Analysis of bandpassed MJO indices
- Summary and Conclusions

Background: Version 1

The Madden-Julian Oscillation (MJO) is characterized by

- Pronounced multiscale convective organizations over the Indo-Pacific warm pool region
- Mainly equatorially-trapped, eastward propagating speed of $\sim$ 5-8 m/s
- Irregular periodicity (e.g., $\sim$ 20–90 days)
- Associated westerly wind bursts (WWB) near the Dateline

MJO prediction and predictability are significant research areas

- Major source of tropical sub-seasonal (2 weeks-2 months) predictability (e.g., Lau and Waliser, 2005)
  - Statistical models suggest predictability of 15–20 days
  - Dynamical models suggest predictability of 25–30 days.
- Global influences through tropical-extratropical interactions
- Fundamentally interfacing the short-term weather prediction (I.C. problem) and the very long range climate prediction (B.C. problem).

- GCM or NWP models have major difficulties in simulating MJO, and appear to be sensitive to model moist, esp. convection and cloud, processes (e.g., Tokioka et al. 1988; Slingo et al., 1996; Wang and Schlesinger, 1999; Maloney and Hartmann, 2001; Lin et al., 2006)
- Multiscale modeling and global cloud-system-resolving modeling appear to be promising forecast tools (e.g., Miura et al., 2007; Kharioutdinov et al., 2008; Tao et al., 2009)
- Minimal coupled nonlinear oscillator model predicted the system's main features (Majda and Stechmann, 2009)

Background: Version 2

- Detecting chaos and understanding the limit of prediction time based on experimental data analyses is an important task in many areas of science and engineering.
- It is often challenging, since experimental/observational data can be very noisy.
- To make the task amenable, an important step is to first reduce noise in the signals.
- When the signals are linear, this is a simple task since we have a variety of linear filters to choose from to clean up the data.
- When the signals are nonlinear, and especially chaotic, then the problem becomes highly nontrivial since linear filters severely distort even clean chaotic signals (e.g., Badii et al., 1988) let alone effectively reduce noise from them.

Motivational question

- There have been considerable efforts to standardize observation-based diagnostics for objectively evaluating GCM simulations of the MJO (Waliser et al., 2009; Kim et al., 2009). Several EOF-based MJO indices have been developed for both operational monitoring and research purposes.
- Ding et al. (2010) showed an inconclusive range (3 and 5 weeks) of theoretical potential predictability based on such indices using nonlinear finite-time Lyapunov exponent (NFTLE), and indicated that the discrepancy may be caused by noise contamination.
- **Question**: How can we gain significant insights into the MJO predictability by analyzing the MJO indices?
- **Challenges**: We need to suitably pre-process (i.e., filter) the observational data, then comprehensively characterize the underlying dynamics of the processed data.

MJO indices

- Maloney and Hartmann (1998): Index based on the first two EOFs of the bandpass-filtered (20-80 days) 850 hPa zonal wind averaged 5°S-5°N around the equator.
- Wheeler and Hendon (2004) realtime multivariate MJO (RMM): Index based on the the first two EOFs of combined 850- and 200-hPa zonal winds as well as OLR from 15°S-15°N.
- Tian et al. (2006): Index based on the first extended EOF of the bandpass-filtered (30-90-day) rainfall anomalies.
- Xue et al. (2002) and Gottschalck, NOAA CPC MJO indices: Indices based on the first extended EOF of 200hPa velocity potential anomalies from equatorward of 30°N.

Adaptive Denoising Algorithm

- Partition a time series into segments (or windows) of length $2n+1$ points, where neighboring segments overlap by $n+1$ points
- For each segment, fit a best polynomial of order K
- Denote the fitted polynomial for the i-th and $(i+1)$-th segments by $y^{(i)}(l_1),\ y^{(i+1)}(l_2),\ l_1, l_2 = 1, \cdots, 2n+1$, respectively.
- Combine the trends in the overlapped region to obtain

$$y^{(c)}(l) = w_1 y^{(i)}(l+n) + w_2 y^{(i+1)}(l), \quad l = 1, 2, \cdots, n+1$$

  where $w_1 = \left(1 - \frac{l-1}{n}\right), w_2 = \frac{l-1}{n}$ can be written as $(1 - x/n)$, where x denotes the distances between the point and the centers of the two fitted curves
- The trend is smooth at the non-boundary points, and has at least the right- or left-derivative at the boundary points

Choosing the parameters K and w when the true signal is unknown

- w can not be greater than 1/2 of a local period of the variation of the signal, if one does want to trace out the detailed variations of the signal.
- When the signal is highly nonlinear, then $K \leq 2$; however high-order polynomials may not be well defined when w is small.
- Fix K to be 2, then check how the variance of the residual data varies with w; a generic pattern is that the variance
  1. increases with w when w is small (almost perfect fitting, little denoising)
  2. flattens out when w keeps increasing (usually desired)
  3. increases sharply again when w is further increased (window size too big, local variations largely removed)
- Increase K until the above pattern changes little.

Denoising

- Chaotic Lorenz '63 model:

$$\begin{aligned} \dot{x} &= -10(x-y) + D_1\eta_1(t), \\ \dot{y} &= -xz + 28x - y + D_2\eta_2(t), \\ \dot{z} &= xy - \tfrac{8}{3}z + D_3\eta_3(t), \end{aligned} \tag{1}$$

- Measurement noise: $x(t)+n(t)$; $RMSE = \sqrt{\frac{1}{N}\sum_{i=1}^{N}[x(i)-\hat{x}(i)]^2}$
- Dynamical noise: noise is in the equations of the system ($D_i \neq 0$); *RMSE* cannot be defined; effectiveness of denoising can be evaluated through recovery of chaotic signatures
- Experimental data: both measurement and dynamical noise may exist; *RMSE* cannot be defined

Denoising of the Lorenz model

Chaotic Lorenz ’63 model with measurement noise

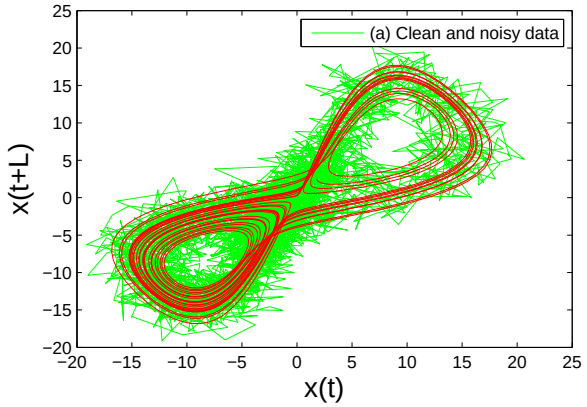

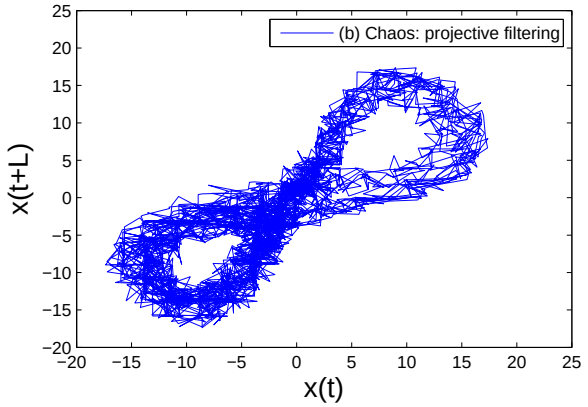

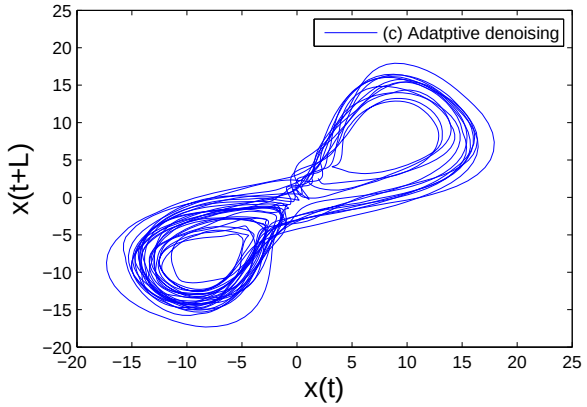

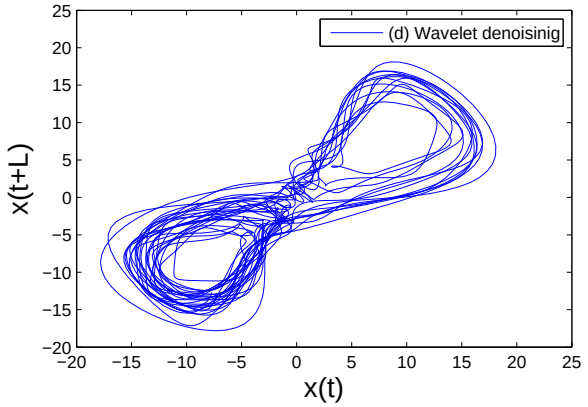

Denoising of chaotic Lorenz data: performance

- Badii et al. *Phys. Rev. Lett.* 1988: linear filtering is not suitable for chaotic data
- Adaptive denoising can more effectively reduce both measurement and dynamical noise than chaos and wavelet based approaches (and therefore, is the most effective)

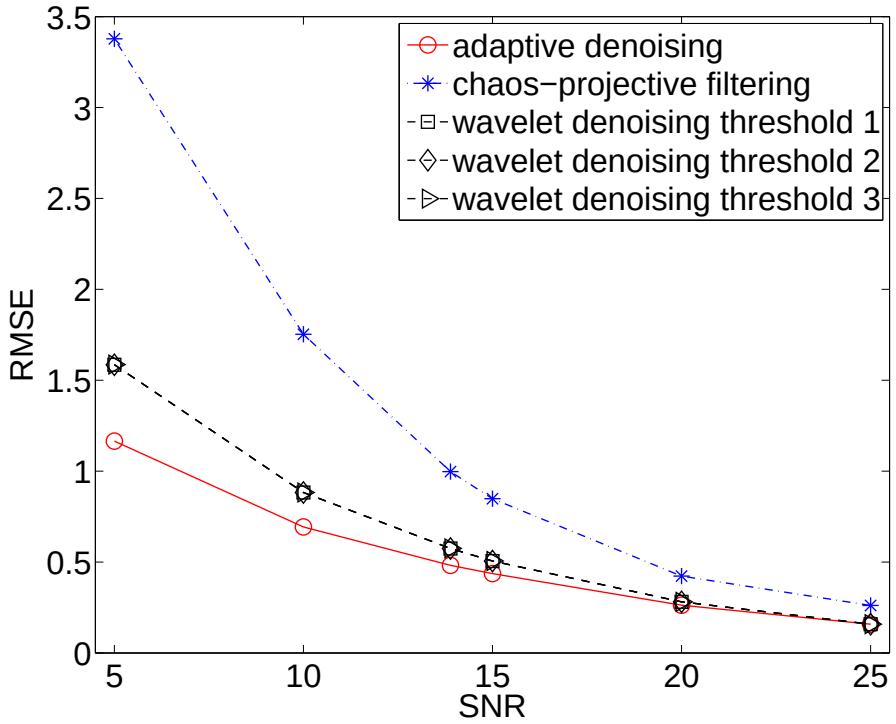

Recovered chaotic signatures

Fractal dimension (correlation dimension D_2, Grassberger-Procaccia, 1983) and the Scale-Dependent Lyapunov Exponent (SDLE, Gao et al. 2007)

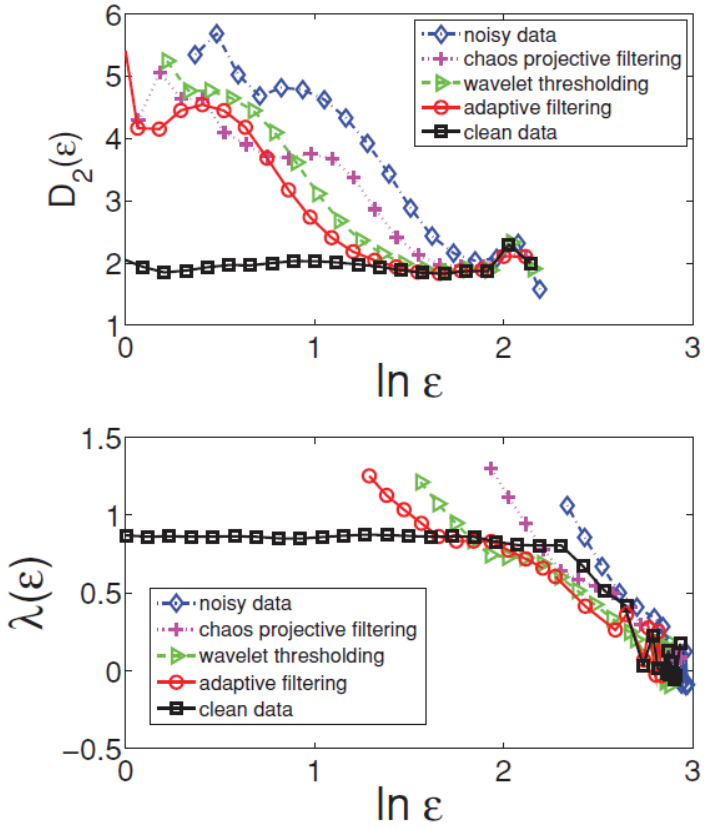

NOAA CPC pentad MJO indices

- Extended Empirical Orthogonal Function (EEOF) analysis is applied to pentad 200-hPa velocity potential (χ_{200}) anomalies equatorward of 30^oN during ENSO-neutral and weak ENSO winters (November-April) in 1979-2000.
- The first EEOF is composed of ten time-lagged patterns.
- Ten MJO indices are the minus projection of the pentad χ_{200} anomalies onto the ten time-lagged patterns of the first EEOF of pentad CHI200 anomalies.
- Anomalies are based on the 1979-1995 period, and each index is normalized by its standard deviation during ENSO-neutral and weak ENSO winters (November-April) in 1979-2000.
- The blueish (reddish) color represents the enhanced (suppressed) convection, and the x-axis labels the centers (20^oE, 70^oE, 80^oE, 100^oE, 120^oE, 140^oE, 160^oE, 120^oW, 40^oW and 10^oW)

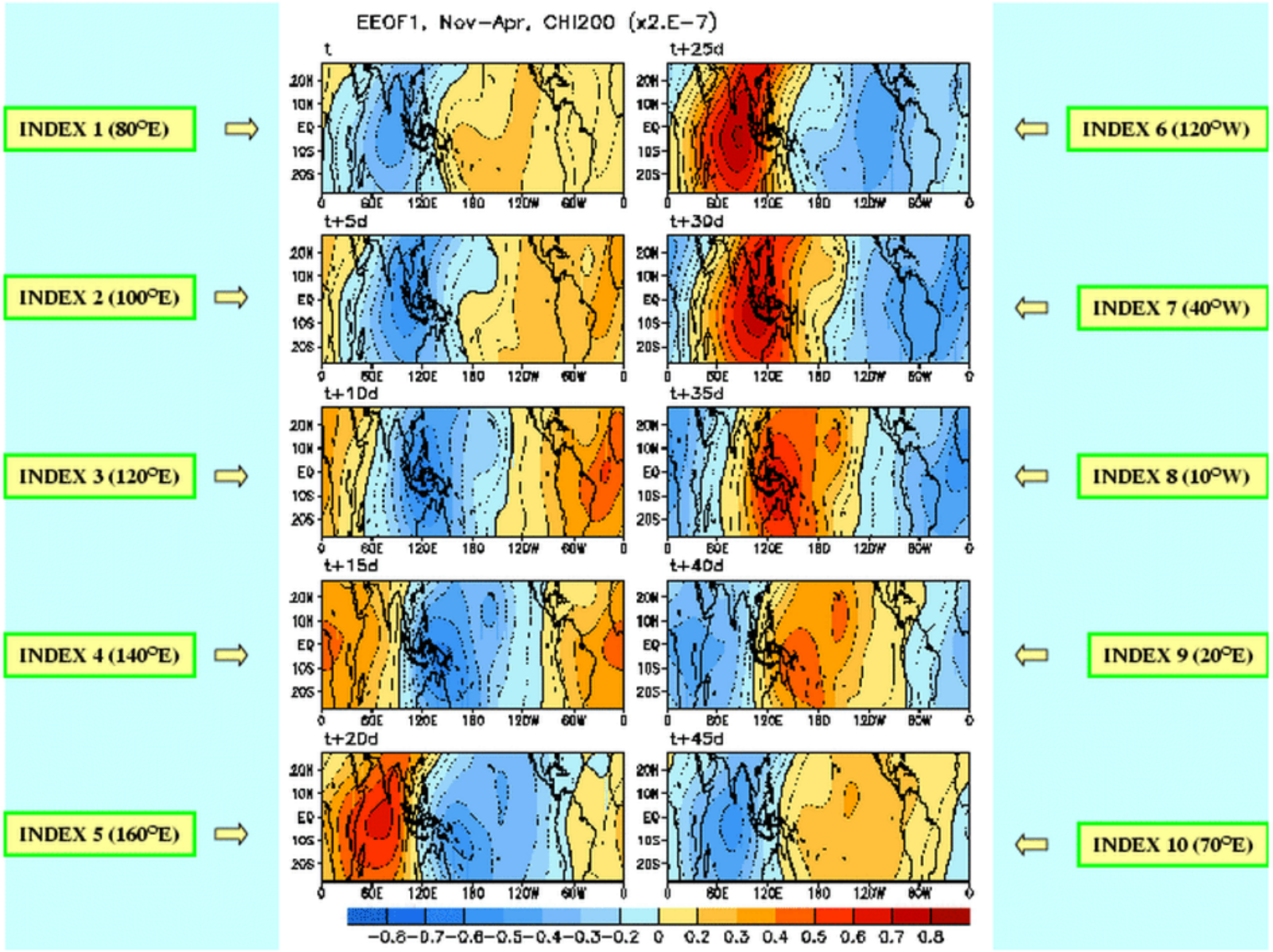
EEOF1, Nov–Apr, CHI200 (x2.E–7)
t
t+25d
t+5d
t+30d
t+10d
t+35d
t+15d
t+40d
t+20d
t+45d
INDEX 1 (80°E)
INDEX 2 (100°E)
INDEX 3 (120°E)
INDEX 4 (140°E)
INDEX 5 (160°E)
INDEX 6 (120°W)
INDEX 7 (40°W)
INDEX 8 (10°W)
INDEX 9 (20°E)
INDEX 10 (70°E)
20N
10N
EQ
10S
20S
0
60E
120E
180
120W
60W
−0.8 −0.7 −0.6 −0.5 −0.4 −0.3 −0.2 0 0.2 0.3 0.4 0.5 0.6 0.7 0.8

Pre-processing MJO index data (at 80°E)

- The NOAA CPC pentad MJO indices from 1978–present.
- Green and red curves: window sizes 33 and 11 (∼82.5 and 27.5 days)
- Focus of further analysis: bandpassed signal
  (27.5 to 82.5 days; 82.5 days is not an important scale)

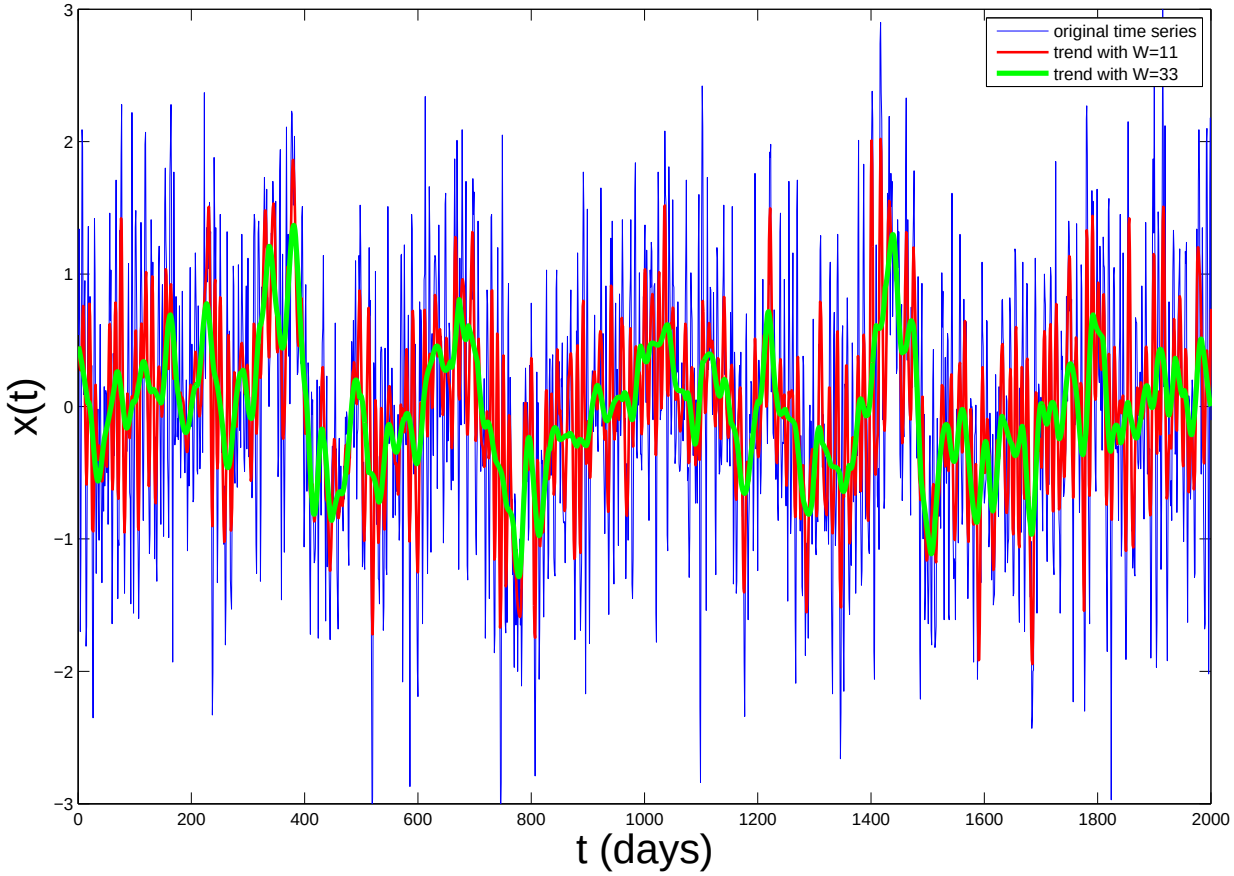

Logarithmic Power Spectral Density (PSD) of MJO index (80°E)

- Bandpass filtering makes the spectral peaks sharper

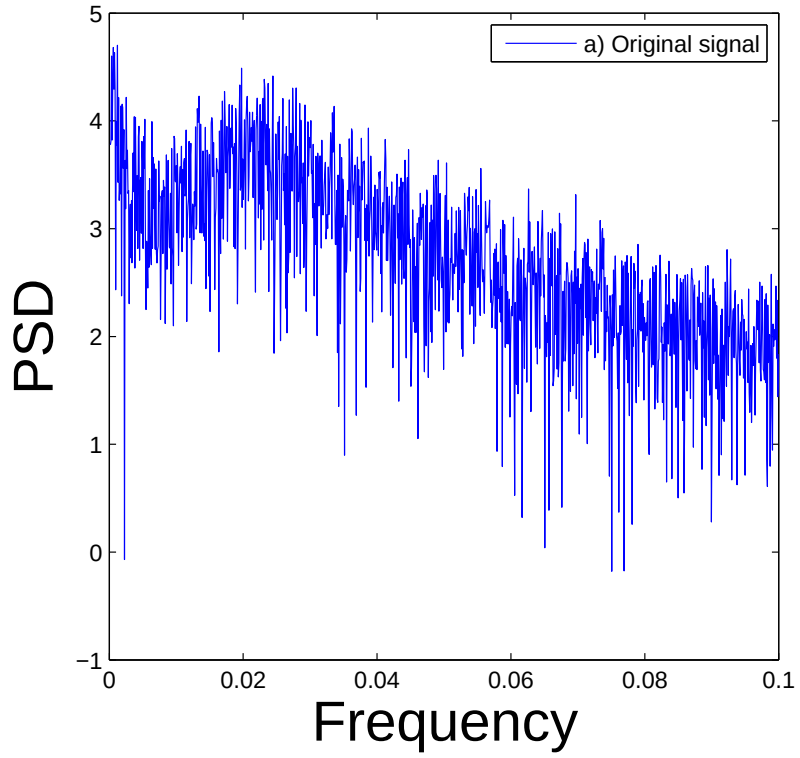

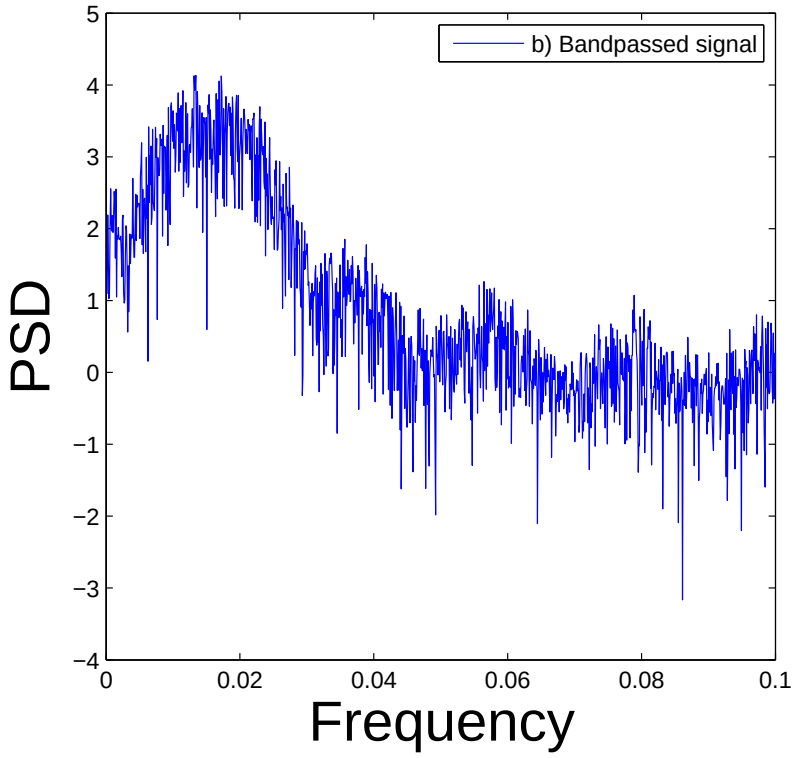

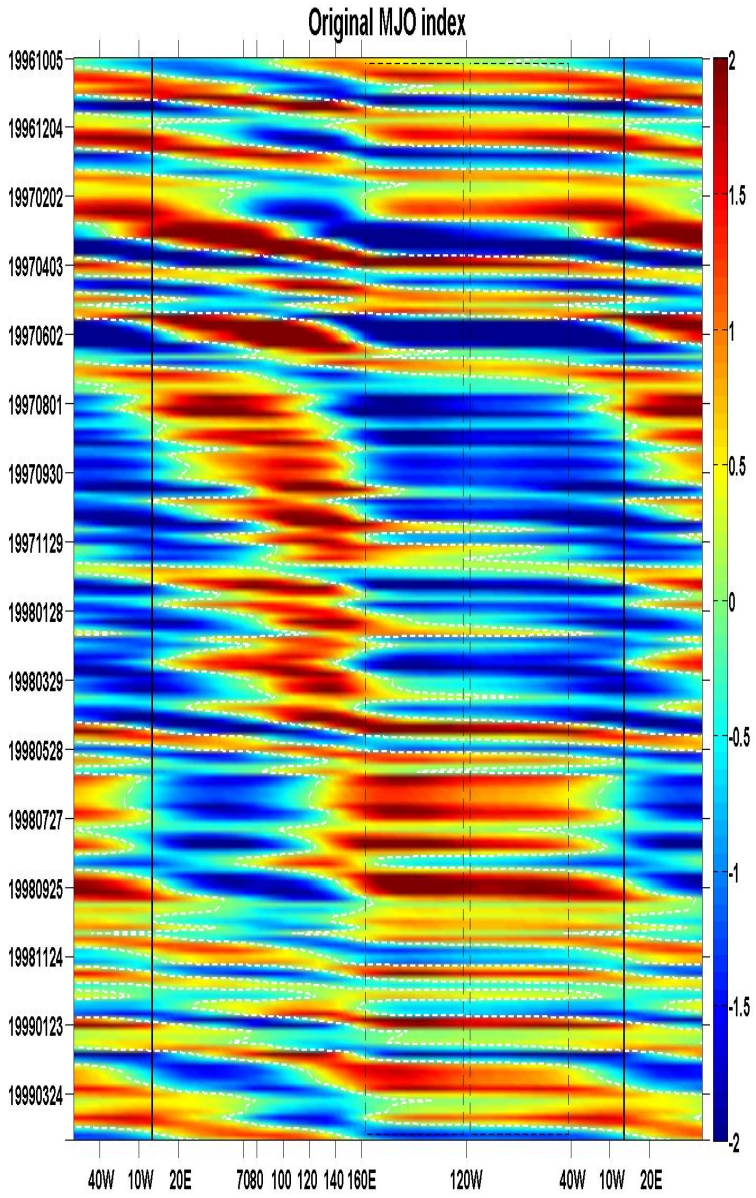
Original MJO index
19961005
19961204
19970202
19970403
19970602
19970801
19970930
19971129
19980128
19980329
19980528
19980727
19980925
19981124
19990123
19990324
40W 10W 20E 7080 100 120 140 160E 120W 40W 10W 20E
2
1.5
1
0.5
0
-0.5
-1
-1.5
-2

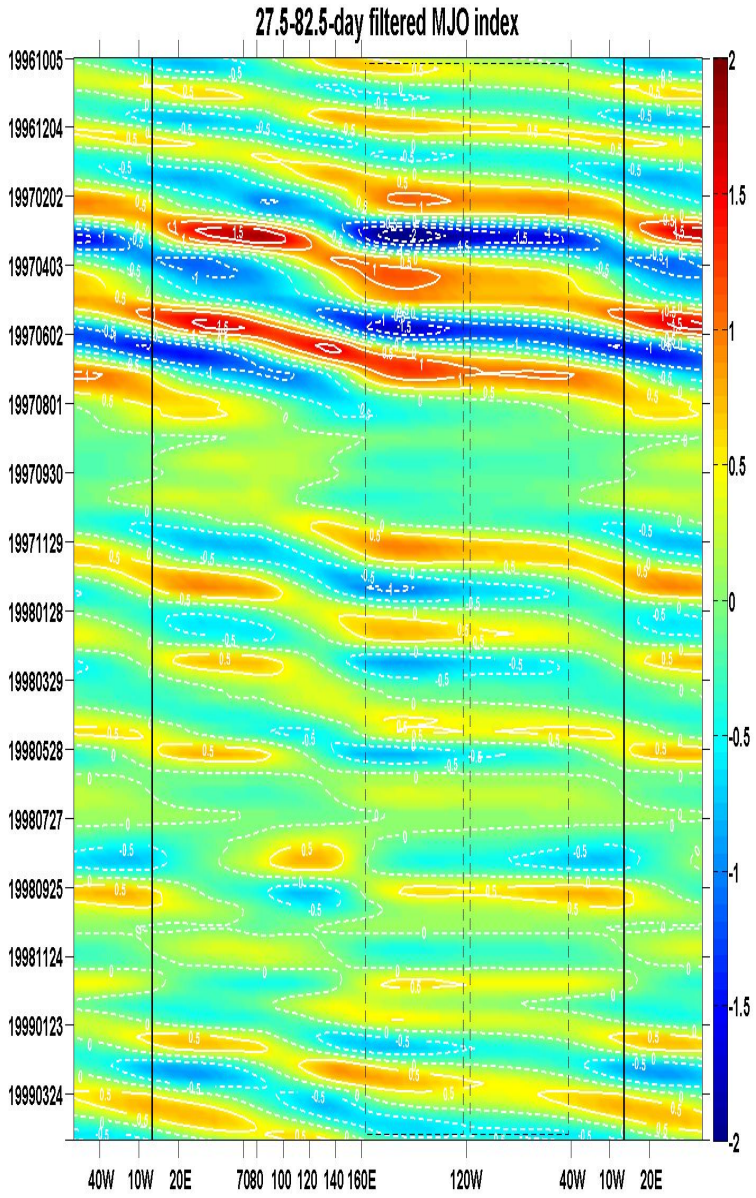
27.5-82.5-day filtered MJO index
19961005
19961204
19970202
19970403
19970602
19970801
19970930
19971129
19980128
19980329
19980528
19980727
19980925
19981124
19990123
19990324
40W 10W 20E 7080 100 120 140 160E 120W 40W 10W 20E
2
1.5
1
0.5
0
-0.5
-1
-1.5
-2

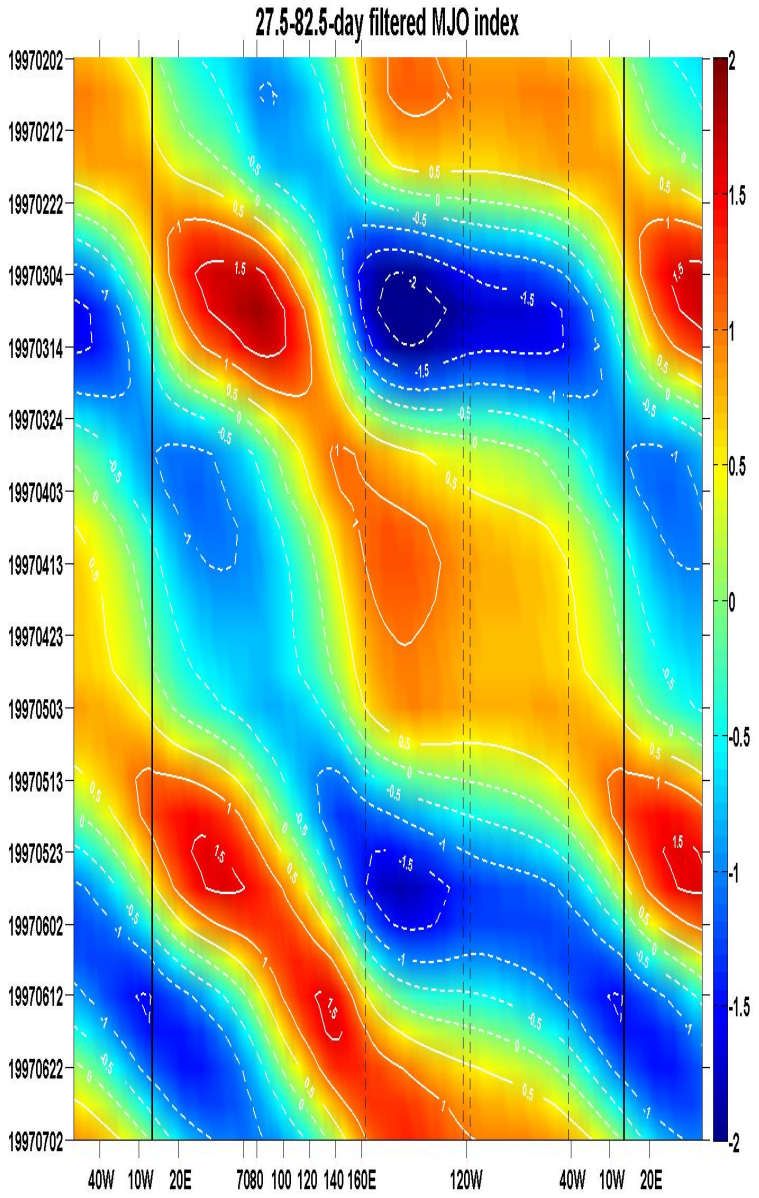
27.5-82.5-day filtered MJO index
19970202
19970212
19970222
19970304
19970314
19970324
19970403
19970413
19970423
19970503
19970513
19970523
19970602
19970612
19970622
19970702
40W 10W 20E 7080 100 120 140 160E 120W 40W 10W 20E
2
1.5
1
0.5
0
-0.5
-1
-1.5
-2

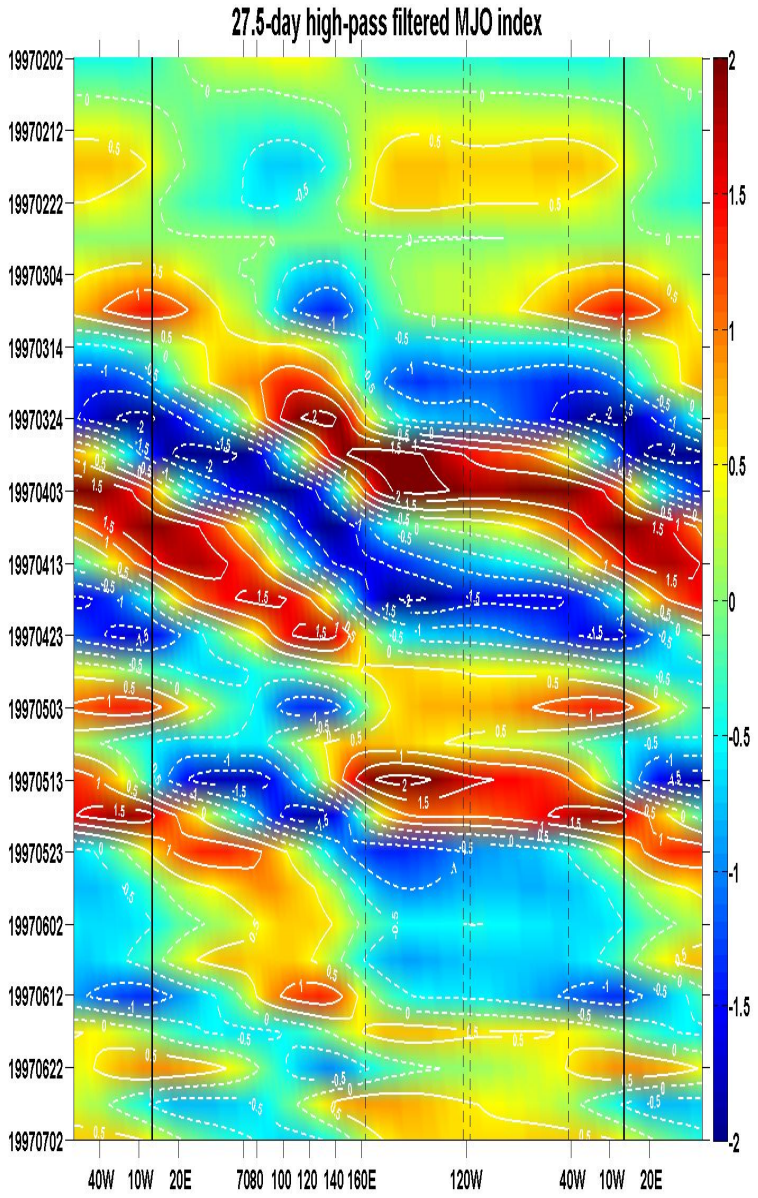
27.5-day high-pass filtered MJO index
19970202
19970212
19970222
19970304
19970314
19970324
19970403
19970413
19970423
19970503
19970513
19970523
19970602
19970612
19970622
19970702
40W 10W 20E 7080 100 120 140 160E 120W 40W 10W 20E
2
1.5
1
0.5
0
-0.5
-1
-1.5
-2

Phase diagram for bandpassed MJO index data

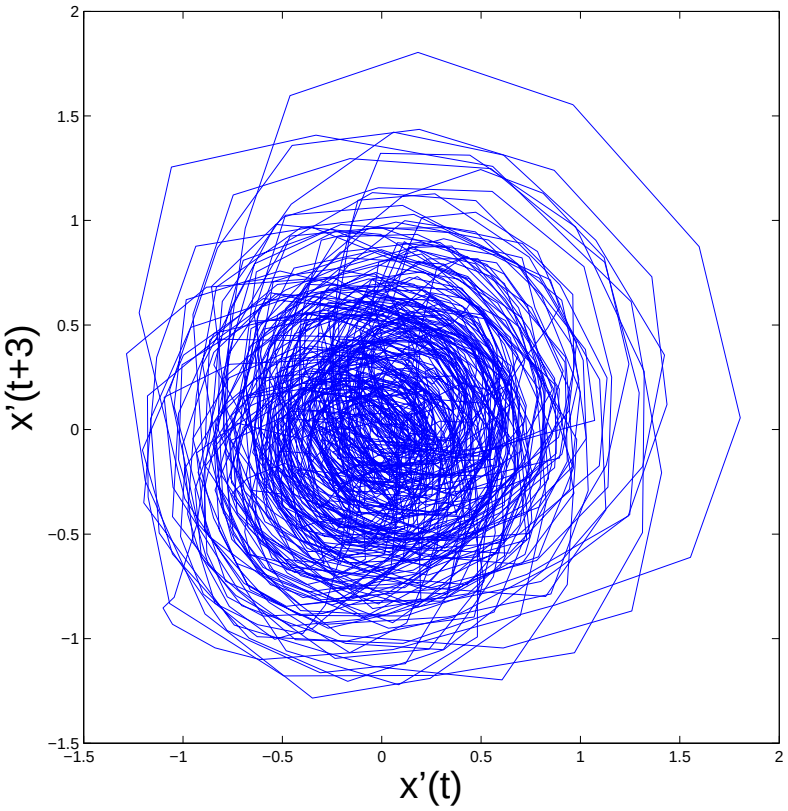

- To obtain the phase space (i.e., a circle) of a harmonic oscillator from a signal $x(t) = sin\omega t$, one may plot $x(t+L)$ against $x(t)$, with $L =$ $1/4$ of the period of the motion
- The plot suggests a circular (oscillatory) motion with period close to $3 \times 5 \times 4 = 60$ days
- The amplitude of the motion varies considerably
- Question: Is the motion regular or chaotic?

Basics of chaos theory

- Chaos also called strange attractor
- Being an attractor, trajectories in the phase space bounded
- Being strange, nearby trajectories diverge exponentially fast: $dr \sim dr_0 e^{\lambda_1 t}$, λ_1: the largest positive Lyapunov exponent
  —**Sensitive dependence on initial conditions**
- A strange attractor typically is a fractal—non-integer dimension
- Popular test for chaos:
  Positive Lyapunov exponent + non-integer fractal dimension
  — False-alarm example: The $1/f^{2H+1}$ process with Hurst parameter H has a fractal dimension $1/H$
- **Key**: a unifying tool to classify various types of processes: to identify different scale ranges where different types of processes are manifested
  — Scale-Dependent Lyapunov Exponent (SDLE)

Characterizing chaos by the scale-dependent Lyapunov exponent (SDLE)

(e.g., Gao, Cao, Tung, and Hu, 2007)

- Consider an ensemble of trajectories in **phase space**
- Denote the initial separation between two nearby trajectories by ε_0, and their **average separation** at time t and $t+\Delta t$ by ε_t and $\varepsilon_{t+\Delta t}$, respectively
- Being defined in an average sense, ε_t and $\varepsilon_{t+\Delta t}$ can be readily computed from any processes, even if they are non-differentiable
- When $\Delta t \to 0$, SDLE $\lambda(\varepsilon_t)$ is defined by

$$\varepsilon_{t+\Delta t} = \varepsilon_t e^{\lambda(\varepsilon_t)\Delta t} \qquad \text{or} \qquad \lambda(\varepsilon_t) = \frac{\ln \varepsilon_{t+\Delta t} - \ln \varepsilon_t}{\Delta t}$$

- Equivalently, we have a differential equation for ε_t,

$$\frac{d\varepsilon_t}{dt} = \lambda(\varepsilon_t)\varepsilon_t$$

- $1/\lambda(\varepsilon_t)$ amounts to the error doubling time
  — larger doubling time means longer prediction time scale

SDLE $\lambda(\varepsilon)$ for chaos, noisy chaos, & noise-induced chaos

- Chaos: $\lambda(\varepsilon) \approx \lambda_1 = \text{const}$ (largest positive Lyapunov exponent)
- Noisy chaos & noise-induced chaos: $\lambda(\varepsilon) \sim -\gamma \ln \varepsilon$ on small scales
- (i) Stochastic Lorenz ('63) system (e.g., Tung et al., 2009)
  (ii) Noisy logistic map
  $x_{n+1} = \mu x_n(1-x_n) + P_n, 0 < x_n < 1, \mu = 3.74, \sigma_{P_n} = 0.002$
  —without noise, motion is periodic — Noise-induced chaos

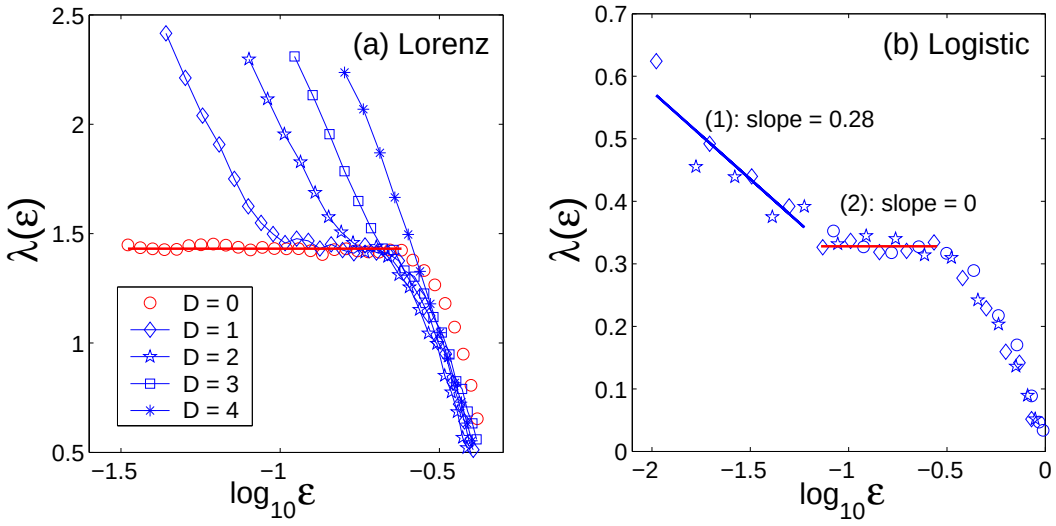

Power-law scaling of $\lambda(\varepsilon)$ for $1/f^{2H+1}$ processes

Can prove $\lambda(\varepsilon) \sim \varepsilon^{-1/H}$

For ON/OFF intermittency, $H = (3-\mu)/2$

Similar power-law scaling for Levy processes

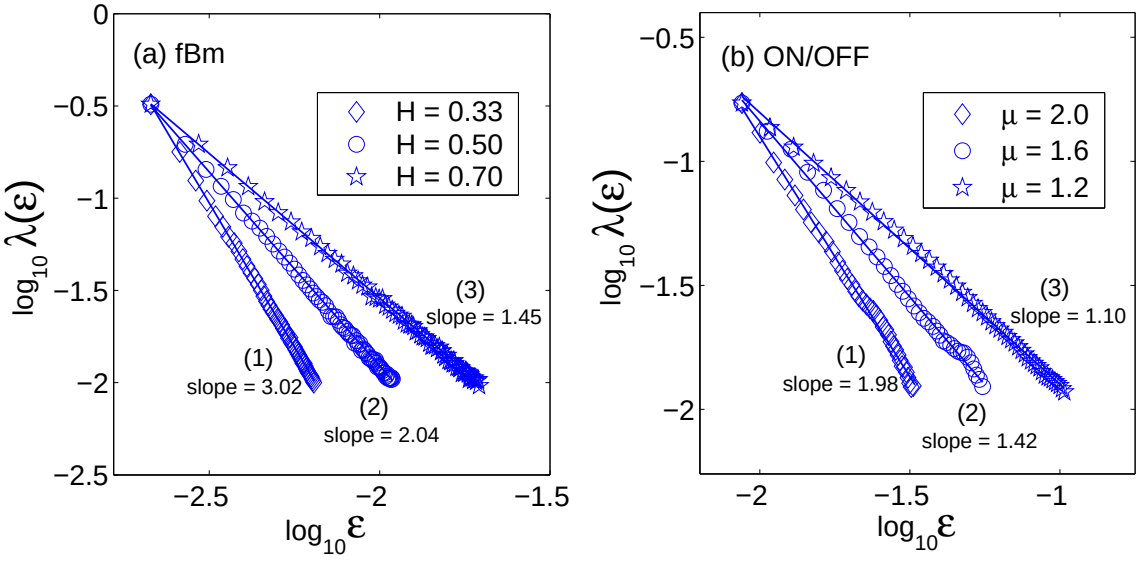

Detecting intermittent chaos

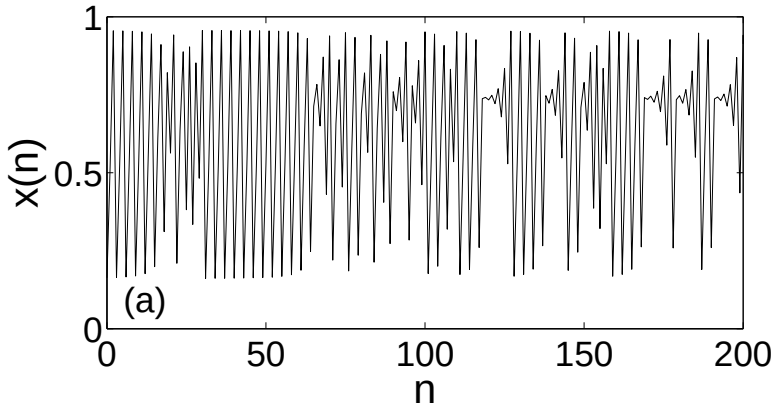

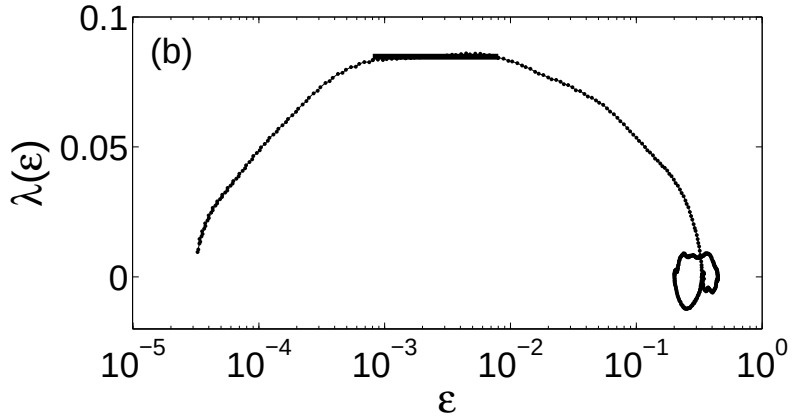

- Intermittent chaos: regular and chaotic motions co-exist; chaotic phase can be much shorter than regular phase
- Very difficult to characterize
- Existing methods cannot detect such motions from noisy time series
- SDLE easily works, due to scale separation property
- Example: logistic map
  $x_{n+1} = a x_n (1 - x_n),\ a = 3.8284$

Physical significance of the SDLE

- $1/\lambda(\varepsilon)$ amounts to the error doubling time
  — larger doubling time means longer prediction time scale
- The first estimate of the doubling time in GCM was 5 days, given by the Mintz-Arakawa two-layer model (Charney et al. 1966)
- With greater computational power and model complexity, one would expect doubling time to increase; however, the estimate of the doubling time has been decreasing
  - A recent estimate (Simmons & Hollingsworth, 2002): < 2 days
- Lorenz suggests that the major factor for the decrease of the doubling time has been the decrease in spatial resolution which introduces finescale uncertainty
- ε is closely related to spatial resolution; when ε decreases, both $\lambda(\varepsilon) \sim -\ln\varepsilon$ and $\lambda(\varepsilon) \sim \varepsilon^{-1/H}$ diverges
  — they are more relevant to reality

The Pseudo-Ensemble Technique

(Gao, Tung, and Hu, 2009)

Essence: ensemble forecasting equivalent based on one time series

- Define a sequence of "shells" indexed as k:

$$\varepsilon_k \leq \|V_i - V_j\| \leq \varepsilon_k + \Delta\varepsilon_k,\ |i-j| > w,$$

where V_i, V_j are vectors sampled from a single trajectory, or vectors reconstructed from a time series $x_1, x_2, \cdots$ using Taken embedding theorem,

$$V_i = [x_i, x_{i+L}, \cdots, x_{i+(m-1)L}],$$

where m and L are embedding dimension and delay time, respectively

- Computation of the SDLE

$\lambda(\varepsilon_t) = \left\langle \ln \|V_{i+t+\Delta t} - V_{j+t+\Delta t}\| - \ln \|V_{i+t} - V_{j+t}\| \right\rangle / \Delta t,$

where the angle brackets denote average within a shell

- Can prove

$\int_0^t \lambda(\varepsilon_t) dt = \Lambda(t) = \left\langle \ln \|V_{i+t} - V_{j+t}\| - \ln \|V_i - V_j\| \right\rangle = \ln \varepsilon_t - \ln \varepsilon_0$

$\Lambda(t)$: Time-dependent exponent (TDE) curves (Gao & Zheng, 93,94)

It's pseudo because all the vectors are from the single trajectory or time series

Prediction in the Lorenz '96 model

- The model is supposed to represent a 1-D atmosphere; F is a positive constant, t is (non-dimensional) time, and X_n are values for some scalar atmospheric quantity on N equally spaced latitude circle

$$dX_n/dt = -X_{n-2}X_{n-1} + X_{n-1}X_{n+1} - X_n + F, \quad n = 1, 2, \cdots, N$$

- $N = 40, F = 8$ are chosen here; there are 13 positive Lyapunov exponents, $D \approx 27.1$
- Can extrapolate to small scales to recover information not resolved by a single dataset

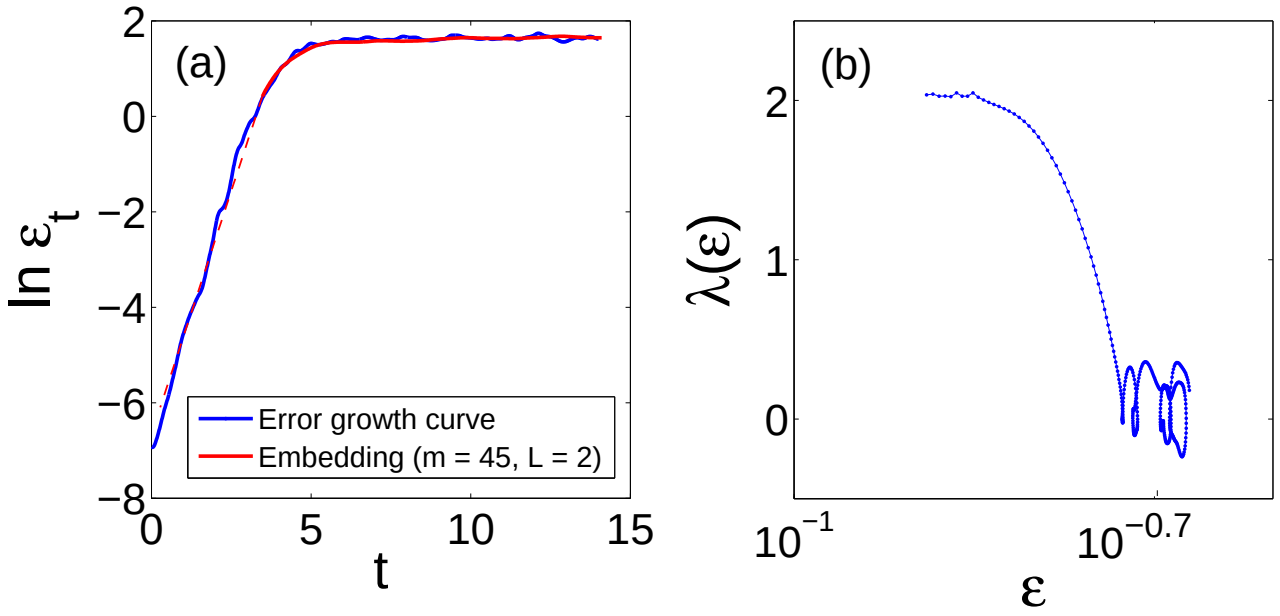

Predictability of MJO (80°E): original data

- SDLE plot does not show any structure
  — suggesting noisy dynamics
- Prediction time is $\sim$ 20 days, roughly the same as what obtained previously (e.g., Waliser, 2005)

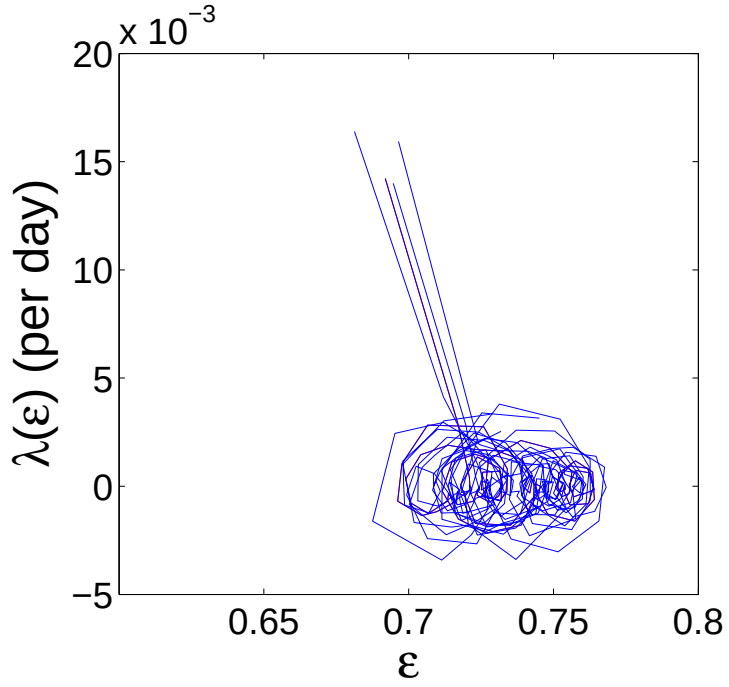

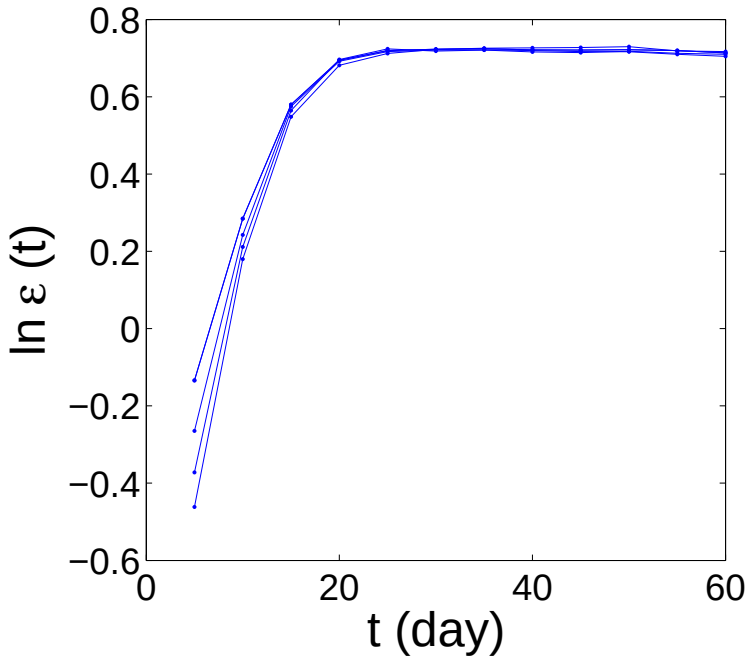

Predictability of MJO (80°E): filtered data

- SDLE plot shows two distinct scalings:
  $\lambda(\varepsilon) \sim -\gamma \ln \varepsilon$ and $\lambda(\varepsilon) \sim \lambda_1 = constant$
- There are two prediction time scales

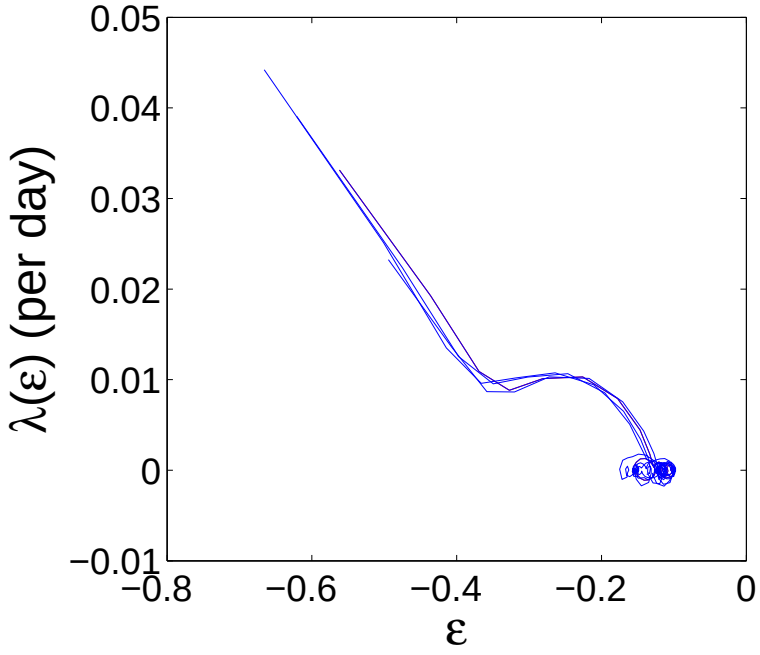

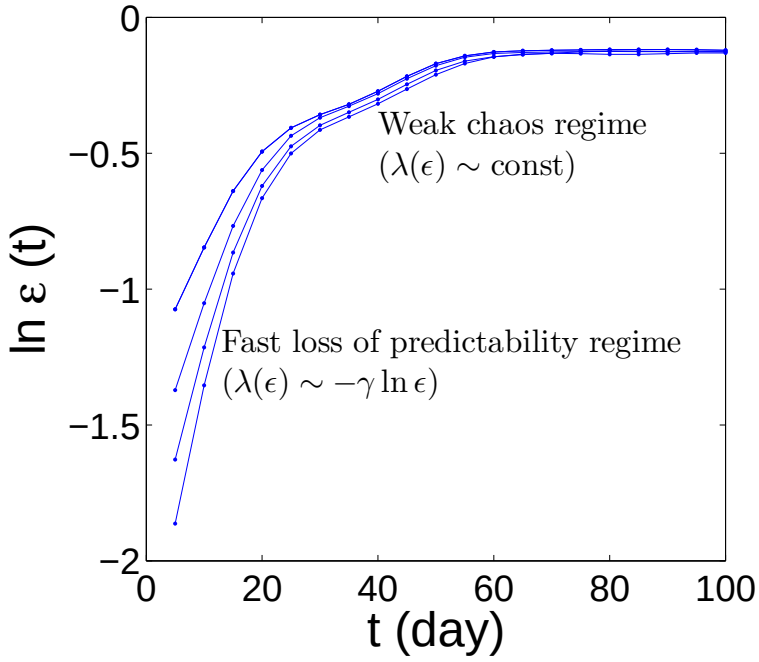

RMM1: filtered data

- There are also two prediction time scales

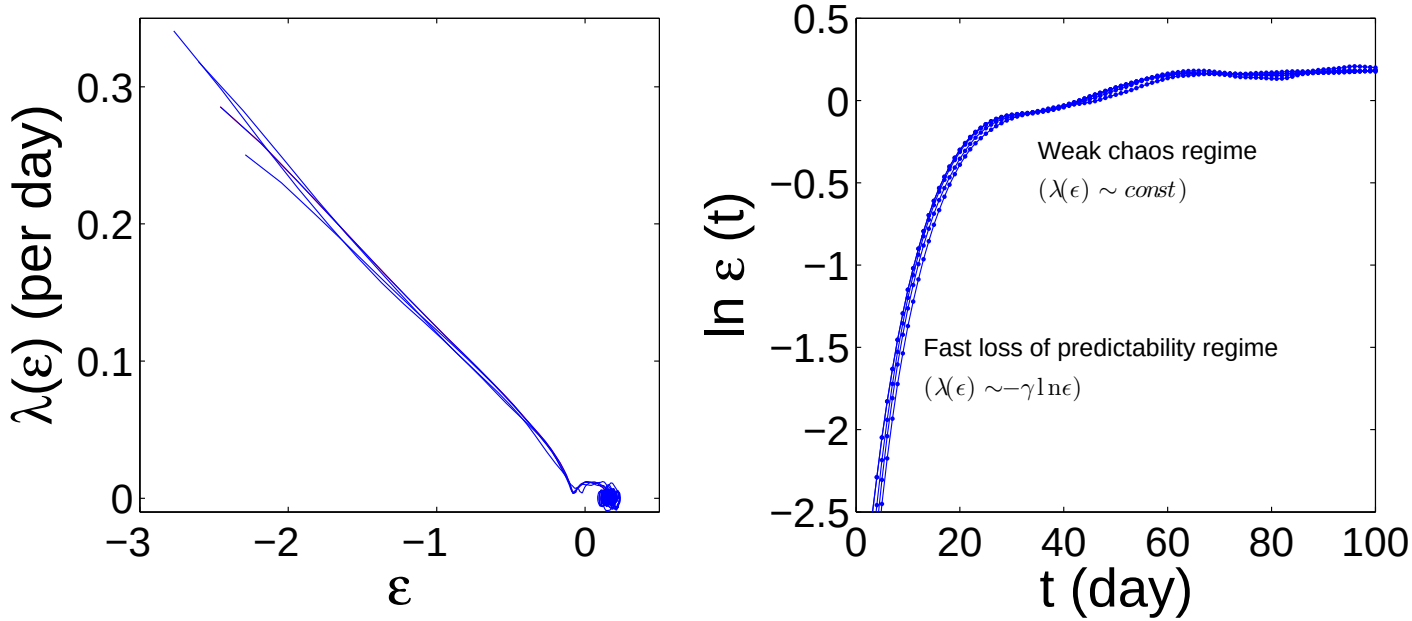

Spatial variability of MJO's predictability

Neither scaling behavior varies much along the longitude

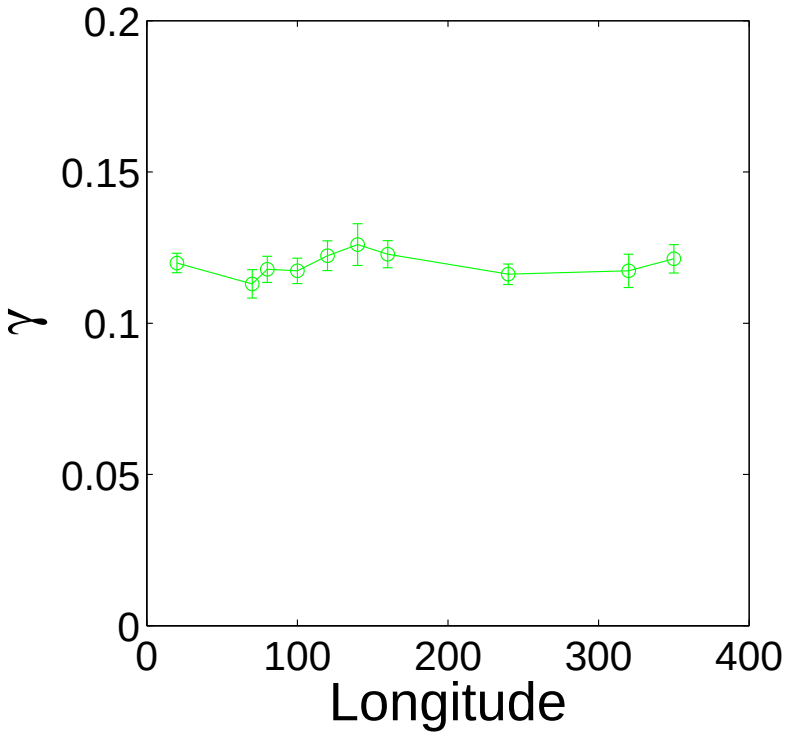

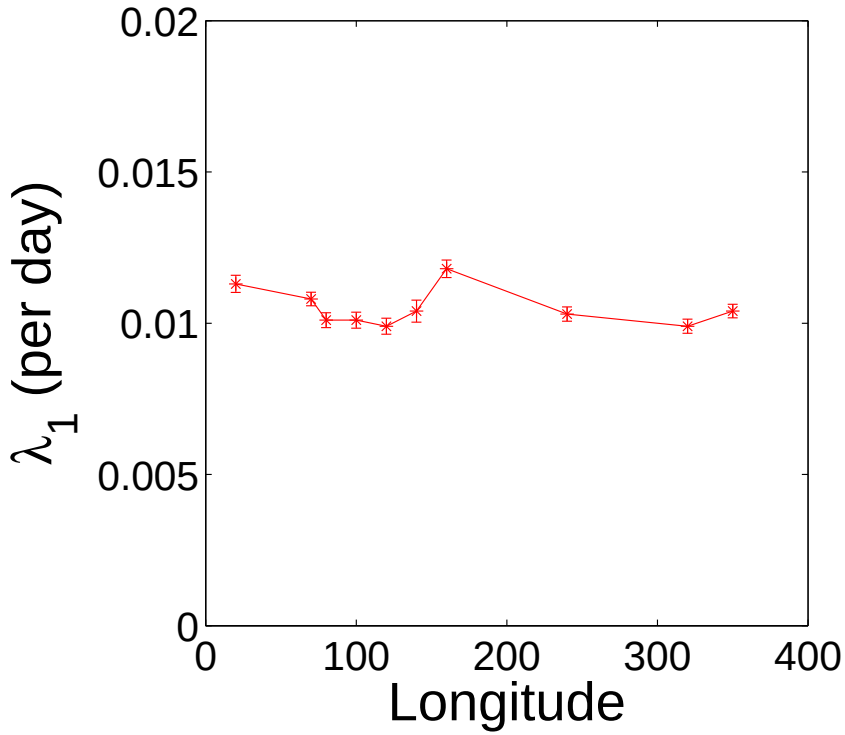

The meaning of chaos and oscillation in MJO?

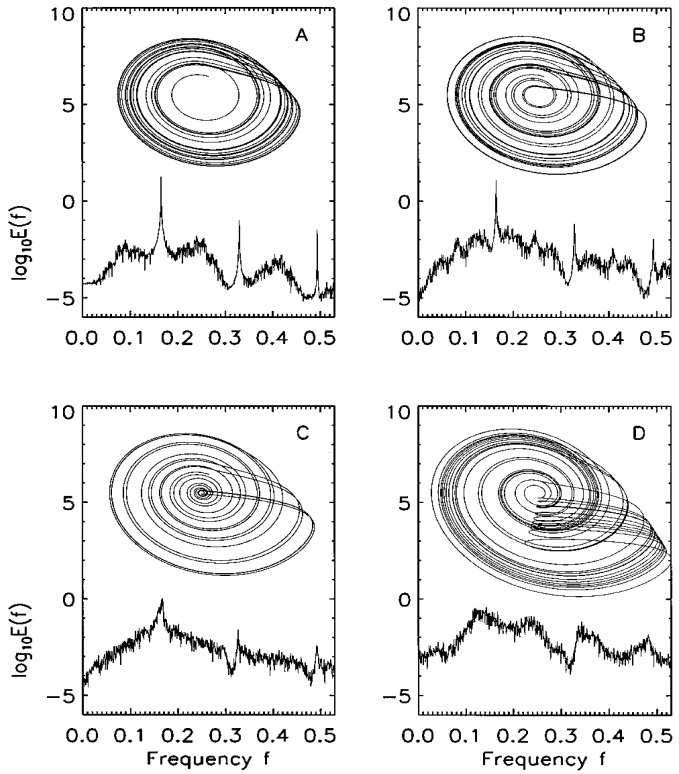

- Chaotic Rossler attractor: sharp spectral peaks weak when phase coherence is gradually lost
- MJO's oscillation comes from phase coherence; its amplitude variation is chaotic driven by stochasticity

Summary and Conclusions

- Without filtering, using SDLE and pseudo-ensemble approach, the raw indices suggest noisy dynamics with predictability of ~ 20 days.
- Suitable bandpass filtering of MJO indices has brought out the MJO features much better; two distinct scaling regions for the bandpassed MJO indices
  - a stochastically driven regime with rapid loss of predictability ($\sim 20-25$ days) (should be cross-examined with the unfiltered data)
  - a weak chaos regime with a prediction time of $\sim 25-30$ days
- These features vary little along the equatorial belt, indicating that MJO is a very coherent event.
- The ~ 50-day predictability is much longer than found by previous studies and is approaching the lifetime of the MJO.
- The CR-GCM or the MMF approach might have simulated the 'stochastic' equivalent better than conventional GCMs for NWP purposes.
- Theoretical models could capture the essence of the MJO dynamics as a stochatically-driven chaotic oscillator and offer fundamental understanding.